

# Low-resolution reflectometry for inline thin-film inspection

Silas I. Ifeanyi<sup>a,\*</sup>, Alex Zheng<sup>a</sup>, Kevin Musselman<sup>a</sup>, Simarjeet Saini<sup>b</sup>

<sup>a</sup>Department of Mechanical and Mechatronics Engineering, University of Waterloo, Waterloo, ON N2L 3G1, Canada; <sup>b</sup>Department of Electrical and Computer Engineering, University of Waterloo, Waterloo, ON N2L 3G1, Canada

## ABSTRACT

High-throughput manufacturing of large-area nano-thin films is critical for displays, batteries, solar cells, and food packaging. However, inline inspection has not kept pace with production speeds, as full-spectrum reflectometry is computationally expensive and sensitive to motion and vibration. This work investigates the feasibility of reduced spectral resolution (multispectral) reflectometry for inline thin-film thickness estimation. Zinc oxide (ZnO) coatings with nominal thicknesses from 4 to 30 nm deposited on polylactic acid (PLA) substrates were characterized using k-nearest neighbors, principal component analysis, and Fourier transform-based regression. The spectral resolution of their reflectance spectra was reduced from 1 nm to 150 nm sampling intervals. We found that inference time per sample decreased by orders of magnitude with reduced spectral resolution, while thickness prediction error remained within nanometer-scale accuracy suitable for process control. Thickness prediction error also remained stable under substrate motion at speeds representative of roll-to-roll manufacturing. These results demonstrate that low-resolution reflectometry is a viable and scalable approach for inline nano-thin film metrology.

**Keywords:** reflectometry, thin films, ZnO, PLA, roll-to-roll, multispectral, inline metrology

## 1. INTRODUCTION

High-throughput manufacturing of large-area nano-thin films is critical for displays, batteries, solar cells, and food packaging.<sup>1,2</sup> These applications demand precise thickness control at the nanometer scale to ensure product quality and performance. However, inline inspection has not kept pace with production speeds, creating a metrology gap in modern manufacturing systems.<sup>1</sup>

Most current inspection solutions use offline sampling or sparse inline measurements at discrete points.<sup>2-4</sup> Full-spectrum reflectometry and ellipsometry provide high accuracy in laboratory settings<sup>3,5,6</sup> but face a significant challenge in high-throughput settings. Traditional approaches acquire hundreds of spectral channels and employ computationally intensive inverse models,<sup>7,8</sup> making real-time, full-area inspection impractical at production line speeds.<sup>1</sup> State-of-the-art practice therefore defaults to point-sample inline checks or offline area mapping, with the highest documented point-sample inline speed reaching 60 m/min<sup>1</sup> (Fig. 1).

Full-spectrum analysis requires development of physics and machine learning models using known reflectance spectra or material constants.<sup>8,9</sup> Traditional thin-film reflectometry relies on analyzing interference patterns that arise from multiple reflections at film interfaces.<sup>10,11</sup> The reflectance spectrum contains periodic oscillations whose frequency is related to the optical thickness (physical thickness times refractive index). Physics-based approaches typically employ transfer matrix methods or Fresnel equation models to fit measured spectra,<sup>5,10</sup> while machine learning methods use spectral databases to train regression models.<sup>2,12</sup> Both approaches face computational costs that scale linearly with spectral resolution. For high-throughput applications demanding sub-second response times across large substrate areas, this computational burden limits the spatial coverage and temporal resolution achievable with conventional metrology systems.<sup>1</sup> Recent work has explored compressed sensing and multi-wavelength approaches,<sup>13</sup> but these still rely on iterative optimization or physics-based inverse models that may be computationally intensive.

---

Further author information: (Send correspondence to Silas I. Ifeanyi)  
Silas I. Ifeanyi: E-mail: sifeanyi@uwaterloo.ca

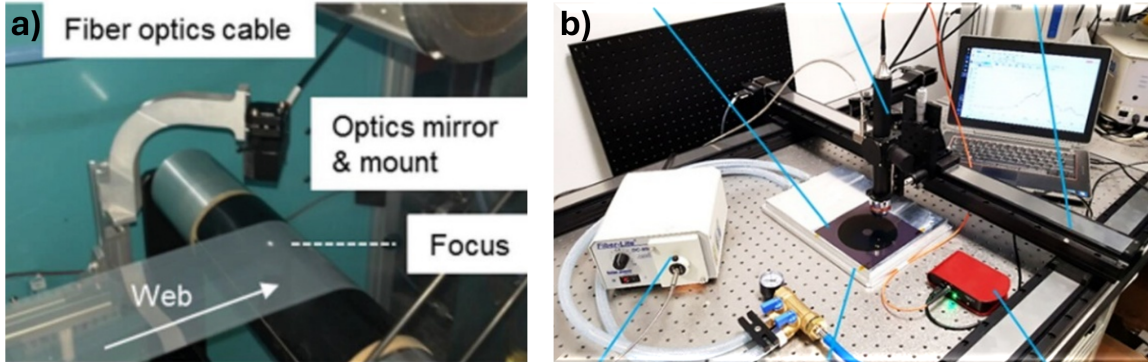


Figure 1. Current reflectance solutions are slow due to full-spectrum analysis, causing users to settle for point-sample inline inspection or offline area mapping. Full-spectrum computation limits throughput, motivating our reduced spectral resolution approach. Adapted with permission from Refs. <sup>1,3</sup>

To tackle the computational bottleneck caused by full-spectra utilization, we use a reflectometry-based thickness characterization that employs reduced spectral resolution. Rather than acquiring full spectra with hundreds of wavelength channels, we evaluate performance using coarsely sampled spectral data – as few as 5 - 15 wavelength bands. Spectral bandwidths of 50nm and 150nm widths were chosen to emulate the bandwidths of commercially available multispectral and rgb camera systems. Three regression models – k-nearest neighbors (kNN), principal component analysis regression (PCA Regression), and Fourier transform-based linear regression (FFT-linear) – are applied to binned reflectance spectra of zinc oxide (ZnO) thin films on polylactic acid (PLA) substrates.

While further exploration is required, our preliminary investigation yielded three key outcomes: First, we demonstrate that inference time decreases by orders of magnitude as spectral resolution is reduced from 1 nm to 150 nm sampling intervals, with sub-millisecond processing achievable at coarse resolutions. Second, the trade-off in prediction error with spectral resolution is modest; 100 nm sampling yields similar root-mean-square error (RMSE) as 1 nm sampling, remaining within  $\pm 5$  nm accuracy suitable for process control. Third, we establish compatibility with industrial environments by showing that thickness inference remains stable under substrate motion at speeds up to 12 m/min, representative of R2R manufacturing conditions. <sup>1,3,14</sup>

This paper is organized as follows: Section 2 describes the experimental apparatus, spectral resolution reduction strategy, and characterization models; Section 3 presents results on computational efficiency, thickness accuracy, and motion robustness; Section 4 discusses observed phenomena, implications for deployment and the limitations of this study; and Section 5 reiterates key findings and future directions.

## 2. METHODS

### 2.1 Samples and Apparatus

Polylactic acid (PLA) substrates with 20  $\mu\text{m}$  thickness were coated with zinc oxide (ZnO) using the well established process of spatial atomic layer deposition. <sup>3,15</sup> Three nominal thickness targets were prepared: 4, 15, and 30nm, representing the range of interest for barrier-film applications. <sup>16</sup> The thickness of the coatings were estimated by using a calculated system growth rate per cycle and number of cycles of Atomic Layer Deposition. <sup>14,17</sup> Four spatially distinct measurement points were selected on each sample to capture within-sample variability.

The measurement apparatus consists of four main components (Fig. 2): (a) a reflectance probe with a bifurcated fiber optic for directing the light to and from the sample; (b) a broadband deuterium-halogen light source (DH-2000, Ocean Insight) covering 200-2500 nm; (c) an OceanHDX spectrometer with about 2068 points from 195-808nm (a native resolution of about 0.30 nm ); and (d) a custom-built translation stage, adapted from a Prusa i3 MK3 3D-printer, enabling controlled substrate motion up to 12 m/min, notably a fraction of roll-to-roll manufacturing speeds.<sup>3</sup>



Figure 2. Measurement apparatus for low-resolution reflectometry: (a) Reflectance probe mounted normally to the surface; (b) DH-2000 deuterium-halogen broadband light source; (c) OceanHDX spectrometer; (d) custom translation stage adapted from a Prusa i3 MK3 3D-printer enabling substrate motion up to 12 m/min.

Reflectance spectra were acquired over the total range of the spectrometer. Integration times were set to 12ms, as it showed acceptable signal-to-noise ratio for our measurements. The spectrometer was calibrated by covering the sensor for dark and using a silicon wafer for "white" reference measurements. The reflectance profile of the silicon wafer was set to 100%. The reflectance profile of the references (dark and "white") were confirmed to correspond to 100% and 0% respectively, every 30mins to ensure the stability of the calibration and illumination conditions, which could drift overtime.<sup>18</sup>

Samples were measured against a matte-black stage to minimize back-side reflections. To take measurements at set speeds (0, 6, 9, and 12 m/min), using G-code the stage was made to oscillate, reaching these speeds mid-oscillation. Each measurement was then taken manually mid-oscillation. Measurements taken outside the sample (indicated by the reflectance spectra) were discarded.

## 2.2 Spectral Preprocessing: Reducing Spectral Resolution and Normalization

To emulate multispectral sensing with reduced channel counts, full-resolution spectra were averaged into uniform wavelength bins (Fig. 3). Five spectral resolutions were evaluated: 1 nm (baseline), 10 nm, 50 nm, 100 nm, and 150 nm sampling intervals. For example, 50 nm binning reduces a 2068-channel spectrum (195–808 nm at 0.3 nm spacing) to 13 channels, representing an almost 200× reduction in data dimensionality.

Binning was performed by averaging all spectral values within each bin, providing a smoothed representation that suppresses high-frequency noise and oscillations from the thicker PLA films.<sup>18,19</sup>

Each binned spectrum was then normalized by dividing the entire spectrum by its intensity value at 300 nm, ensuring all spectra have unit intensity at this reference wavelength. This normalization reduces baseline variations arising from illumination fluctuations.<sup>20</sup>

The binned and normalized spectra constitute the feature vectors for regression modeling. As spectral resolution decreases, the dimensionality of the input feature space decreases proportionally, directly reducing computational load during both training and inference.

## 2.3 Thickness Prediction Models

To ascertain the generalizability of the benefits of spectral resolution reduction, three different types of thickness prediction models were built and evaluated - k-Nearest Neighbors (kNN), Principal Component Analysis Regression (PCA Regression), and Fast Fourier Transform based Linear Regression (FFT-linear). These models were chosen more for their simplicity and interpretability than performance, as a better understanding of their

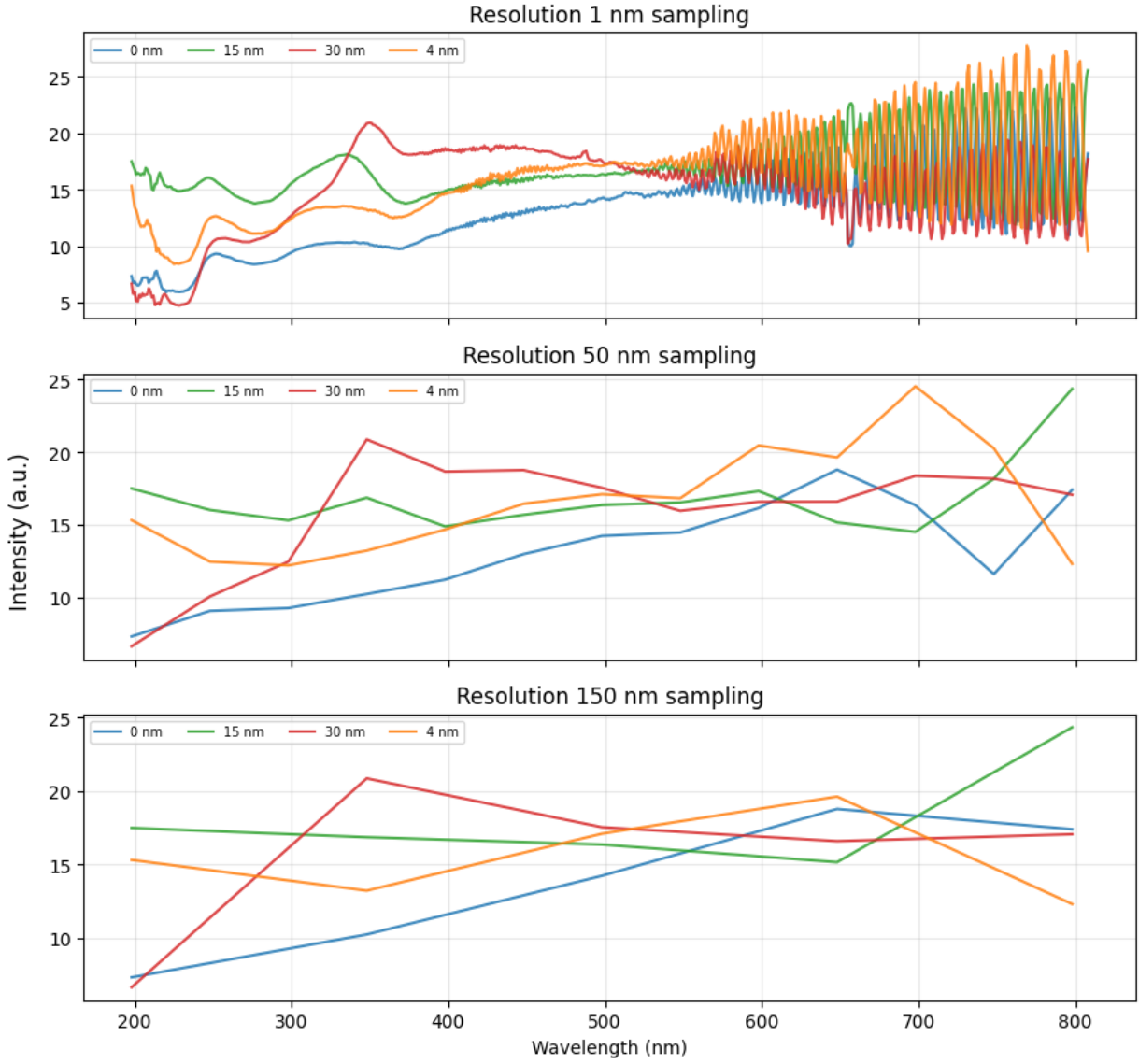


Figure 3. Spectral resolution reduction via uniform wavelength binning. Full-resolution reflectance spectra (1 nm sampling) are averaged into progressively coarser bins (10, 50, 100, 150 nm), reducing dimensionality while preserving thin-film interference features.

underlying mechanisms might help us better understand their interaction with spectral resolution reduction. Further, each model was adapted for each spectral resolution tested. The steps taken to build the models are as follows:

**k-Nearest Neighbors (kNN):** A PLA substrate reference spectrum was constructed by averaging all normalized bare PLA (0 nm coating) measurements, providing a baseline for coating-induced optical changes.

After spectral reduction and normalization, the value of each spectra at 400nm was subtracted from the value of the similarly processed PLA substrate reference. This quantity, called  $\Delta 400$ , meant to capture the changes in the spectra at that wavelength due to the coating thickness, is the feature of interest. The thickness prediction for given spectra is gotten by averaging the thickness values of the samples with the closest  $\Delta 400$  in the training set. For the  $k = 2$  model shown here, two thickness values are averaged. The workflow for this model is shown in Fig. 4a–c.

Table 1. Experimental design matrix showing combinations of spectral resolution, substrate motion, thickness, and regression model.

Variable	Levels	Units	Replicates
Spectral Resolution	1, 10, 50, 100, 150	nm	3
Substrate Velocity	0, 6, 9, 12	m/min	3
Nominal Thickness	4, 15, 30	nm	—
Regression Model	kNN, PCA Regression, FFT-linear	—	—

The Hyperparameters  $k = 2$  and 400nm were selected arbitrarily, but more optimal values could be gotten using cross-validation. More wavelengths can be used in the feature space.

The distance metric operates on the normalized spectral intensities across all wavelength bins. kNN requires no explicit training phase – it is a memory-based method that stores all training examples. Inference involves distance computation and sorting, with complexity  $O(N \cdot D)$  where  $N$  is training set size and  $D$  is spectral dimensionality. As  $D$  decreases with coarser binning, inference time decreases proportionally.

**Principal Component Analysis (PCA):** Normalized spectra are projected onto principal components that capture  $\geq 99\%$  of the total variance in the training set<sup>12</sup> (Fig. 4d–f). Singular value decomposition (SVD) is applied to the centered spectral matrix to identify these components. A linear regression model is then trained to map the reduced-dimensional PC scores to thickness values. PCA reduces sensitivity to noise and collinearity among wavelength channels by concentrating information into orthogonal features. The number of retained components decreases with coarser spectral resolution, as fewer components are needed to explain variance in smoothed data (typically 4–6 components at 50 nm resolution). Training involves SVD and ordinary least-squares fitting; inference requires matrix-vector multiplication with complexity  $O(D \cdot P)$  where  $P$  is the number of principal components ( $P \ll D$ ).

**FFT-linear (Fourier Transform-Based Linear Regression):** Normalized spectra are transformed to the frequency domain via fast Fourier transform (FFT)<sup>21</sup> (Fig. 4g–i). Thin-film interference produces periodic oscillations in reflectance spectra, which manifest as peaks in the Fourier magnitude spectrum. Low-frequency magnitude components (in the case, the first 5) are extracted as features. These features capture the coarser oscillation periods, which are related to optical thickness of the coating, as opposed to the higher frequency oscillations of the thicker substrate. Ordinary least-squares linear regression maps these frequency-domain features to thickness values. FFT computation has  $O(D \log D)$  complexity; for reduced-resolution spectra with small  $D$ , this overhead is negligible, and inference is dominated by the linear transformation, achieving sub-millisecond latency.

All models were trained using 70/30 stratified train-test splits across thickness levels to ensure representative sampling of each coating thickness (0, 4, 15, 30 nm). Training sets included static measurements only; moving-substrate conditions were held out as an independent test set to assess robustness to motion. The PLA reference (0 nm thickness) was constructed from bare substrate measurements and used to establish the baseline optical response. Hyperparameters (kNN neighborhood size, number of PCs retained, frequency components selected) were selected arbitrarily but could be optimized via cross-validation on the training set to prevent overfitting while maximizing prediction accuracy.

## 2.4 Experimental Design and Evaluation Metrics

The experimental design matrix is summarized in Table 1. Variables include spectral resolution (1, 10, 50, 100, 150 nm), substrate velocity (0, 6, 9, 12 m/min), nominal thickness (4, 15, 30 nm), and regression model (kNN, PCA, FFT-linear). Thus far, only specific combinations of variables are shown to illustrate potential trends. A full factorial design that examines all combination is possible.

Performance is quantified using root-mean-square error (RMSE), coefficient of determination ( $R^2$ ), and inference time per sample. For a test set of  $N$  samples with predictions  $\hat{y}_i$  and ground truth  $y_i$ :

$$\text{RMSE} = \sqrt{\frac{1}{N} \sum_{i=1}^N (\hat{y}_i - y_i)^2}. \quad (1)$$

Complete Analysis: Three Regression Approaches (50nm resolution)

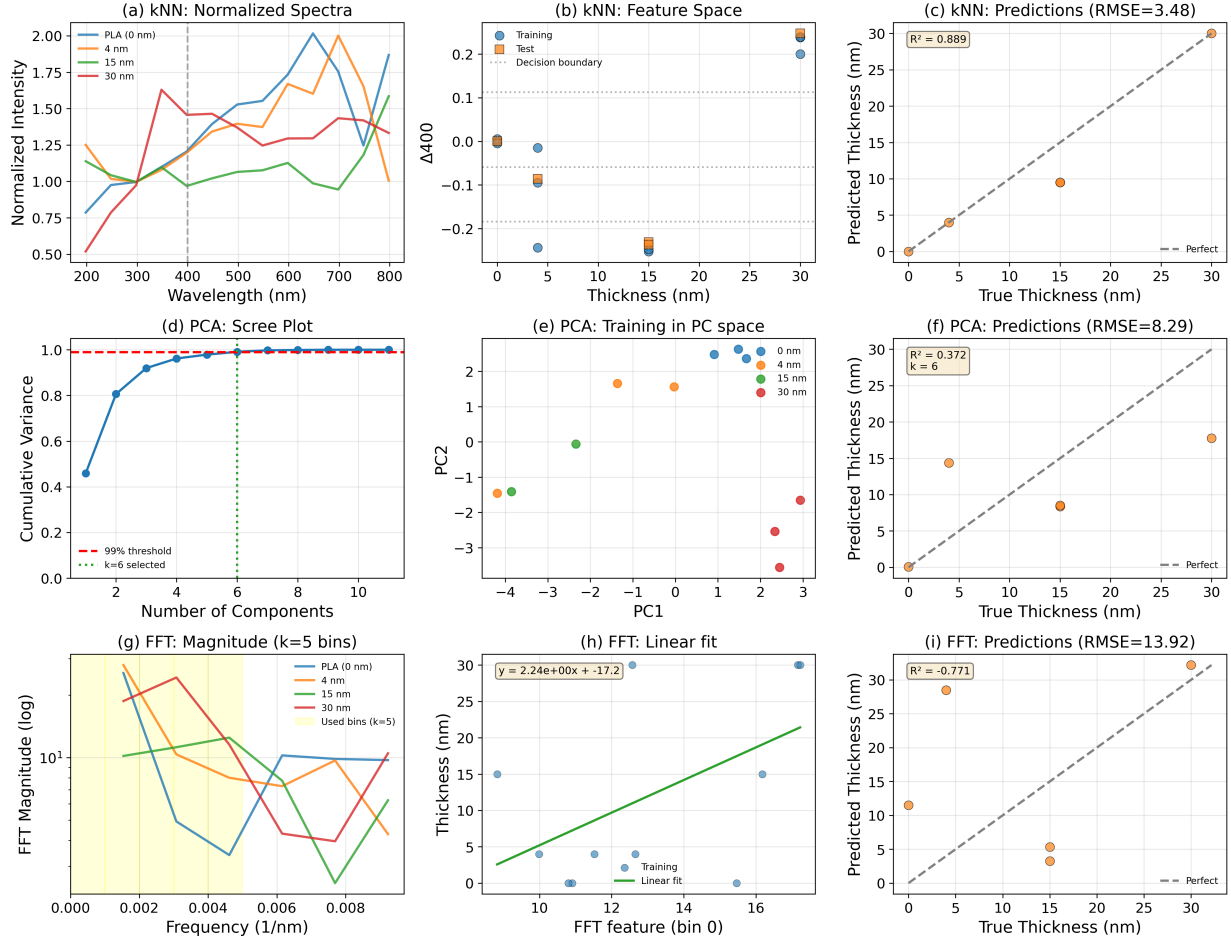


Figure 4. Comparison of three regression approaches for thickness prediction. (a–c) k-Nearest Neighbors (kNN) model workflow: normalized spectra are compared via Euclidean distance, and thickness is estimated by averaging the  $k$  nearest training samples. (d–f) Principal Component Analysis Regression (PCA Regression) workflow: spectra are projected onto principal components capturing  $\geq 99\%$  variance, followed by linear regression on PC features. (g–i) Fourier Transform-Based Linear Regression (FFT-linear) workflow: spectra are transformed to frequency domain, low-frequency magnitude features are extracted, and linear regression maps features to thickness.

Inference time is measured using native python "time" function calls on a standard laptop (Intel i7, 16 GB RAM) which reflects deployment-relevant hardware.<sup>3</sup>

### 3. RESULTS

Figure 5 presents the primary findings across two performance dimensions. Panel (a) shows inference time per sample as a function of spectral resolution for the three regression models. As resolution decreases from 1 nm to 150 nm, inference time drops for all models. At 1 nm resolution,  $\Delta 400$ , which drops the most, requires approximately 0.38 ms per sample but only requires 0.08 ms at 100 nm. The FFT-linear model consistently achieves the fastest inference due to its  $O(D \log D)$  complexity for small  $D$ .

Panel (b) presents RMSE versus spectral resolution for static measurements. At 1 nm resolution, kNN achieves the lowest RMSE of 0 nm. This rises to 3.48 nm for a 10 nm spectral resolution, and stays at that RMSE value until 150 nm. For the PCA Regression model, the RMSE value fluctuates from 7 nm to 11 nm with a slight downward trend. The stability of the models' accuracy across spectral resolutions indicates that

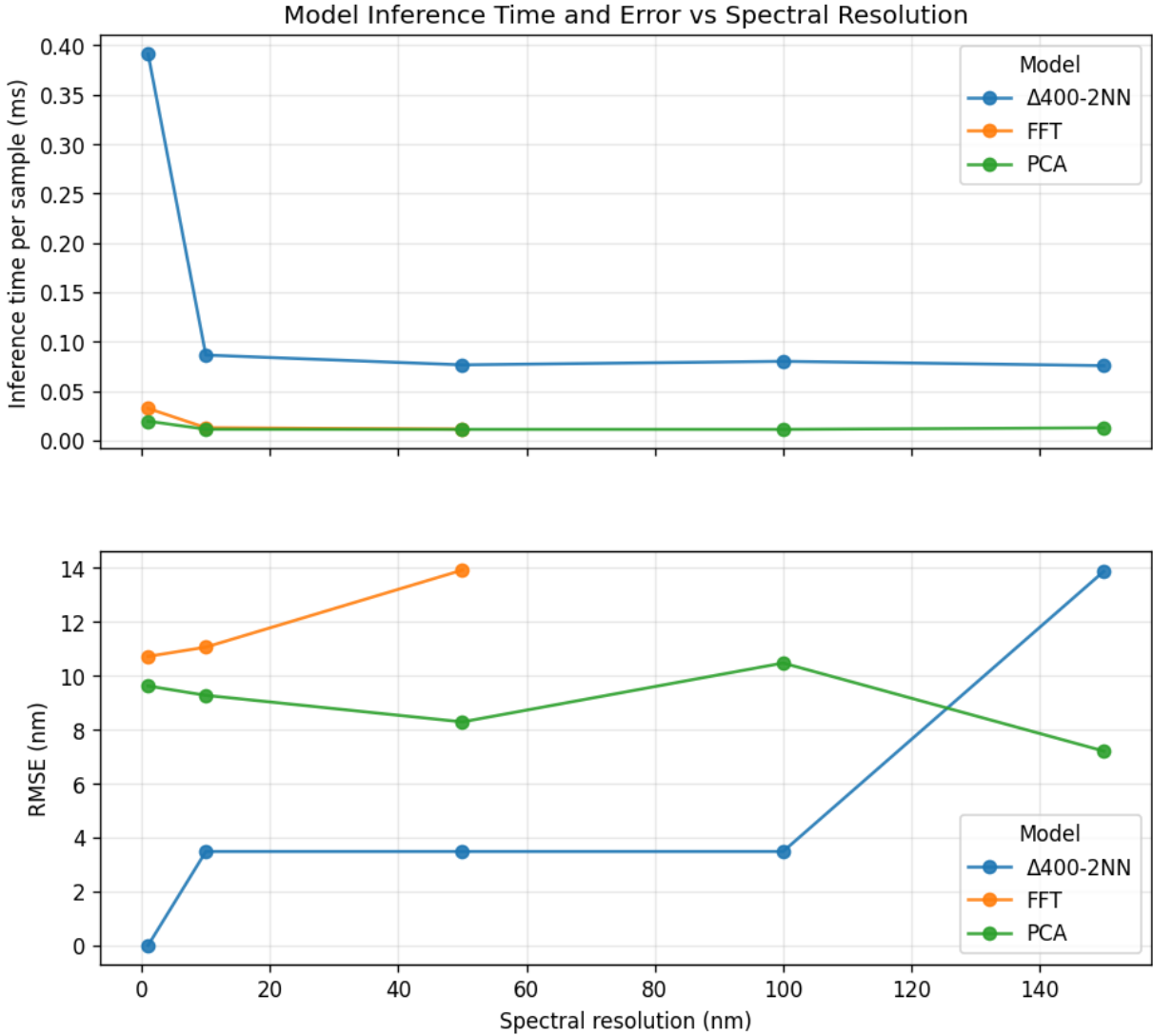


Figure 5. Key results for low-resolution reflectometry: (a) Inference time per sample versus spectral resolution, showing order-of-magnitude reduction as resolution decreases; (b) RMSE versus spectral resolution for static measurements, demonstrating modest accuracy degradation.

reduced-resolution reflectometry can maintain nanometer-scale thickness prediction accuracy suitable for process control. Notably, for some thickness ranges and models, RMSE decreases slightly with coarser binning, likely due to suppression of noise and oscillations from thicker films.<sup>18,19</sup>

Figure 6 demonstrates robustness to substrate motion. RMSE is plotted versus substrate velocity for measurements at 50 nm spectral resolution. Across velocities from 0 to 12 m/min, RMSE remains stable for all models - there does not seem to be a significant downward trend. This stability indicates that motion blur and vibration at production-relevant speeds do not significantly degrade thickness prediction accuracy when integration times are appropriately adjusted (6–24 ms).

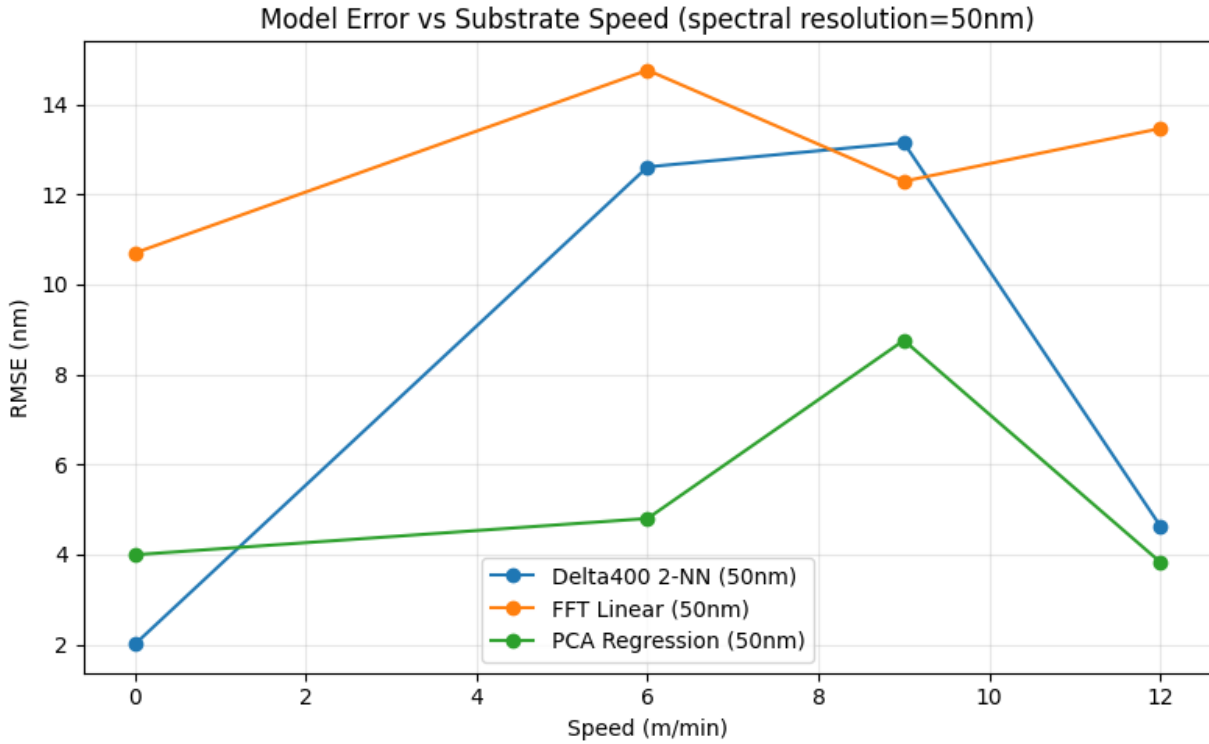


Figure 6. RMSE versus substrate velocity at 50 nm spectral resolution, showing robust performance under motion up to 12 m/min.

#### 4. DISCUSSION

The results demonstrate a favorable accuracy–efficiency trade-off for reduced-resolution reflectometry. This preliminary study may suggest that spectral resolution can be decreased by more than two orders of magnitude (from 1 nm to 150 nm) while maintaining RMSE within acceptable bounds for process control. This finding has significant implications for inline metrology: multispectral sensors with 5–10 discrete wavelength channels can replace full spectrometers, reducing hardware cost, acquisition time, and computational complexity. Further, it enables real-time, full-area inspection at production line speeds, addressing the metrology gap in high-throughput nano-thin film manufacturing.<sup>1</sup>

An unexpected observation is that RMSE decreases in some cases as spectral resolution is reduced, seeming to suggest that low spectral resolution may be better for inspecting nano-thin films. The underlying mechanism behind this might be the suppression of high-frequency noise and oscillations from the thicker PLA substrate, which can obscure the subtle interference patterns from the thin ZnO coatings.<sup>18,19</sup> By averaging over broader wavelength bands, binning effectively smooths the spectra, enhancing the signal-to-noise ratio for thickness-related features. This effect is particularly pronounced for ultra-thin films (4–15 nm) where interference fringe peak widths are broad and low-frequency.

The bands used in this study were selected uniformly for simplicity, but further optimization is possible. Wavelengths can be strategically chosen to maximize sensitivity to thickness variations based on the expected interference patterns.<sup>22</sup> Strategic wavelength selection—choosing bands that coincide with expected interference maxima—could further enhance accuracy for specific thickness ranges.

RMSE also decreases slightly with increasing substrate velocity in some model-resolution combinations. This counterintuitive result may reflect improved spatial sampling: as the substrate moves during integration, the measurement effectively averages over a larger area, reducing the impact of local thickness variations and surface defects. However, the caveat of this benefit is motion blur; at high velocities the spatial location of the measurement becomes uncertain.

Model selection depends on deployment priorities. FFT-linear offers the fastest inference and is suitable for high-throughput applications where sub-millisecond response is required. kNN provides the best accuracy and is preferable when predictive performance is paramount. PCA Regression offers a balance between accuracy and interpretability, as principal components can be analyzed to identify wavelength regions contributing most to thickness estimation.<sup>12</sup>

Limitations of the current study include the sparseness of the dataset used for model training and evaluation. The models were trained and tested on a limited number of samples and thickness levels, which does not allow the models to learn the wavelength-thickness relationship comprehensively. Future work should expand the dataset to include more samples, thickness levels, and substrate materials to improve model generalizability.

Due to the sparseness of the data, statistical significance of the results could not be established. Future work should include more replicates and statistical analysis to confirm the observed trends.

While this work focused on a single material system (ZnO on PLA), the methods used here can be used for other material systems.<sup>2</sup> Generalization to other thin-film materials with different optical constants and interference patterns will require retraining or transfer learning. Future work should address multi-material systems, explore adaptive wavelength selection strategies,<sup>13,22</sup> and validate performance in industrial pilot-scale environments.<sup>3,14</sup>

## 5. CONCLUSIONS

This work establishes the feasibility of low-resolution reflectometry for inline thin-film thickness measurement. By reducing spectral resolution from 1 nm to 50–100 nm, inference time decreases significantly while maintaining RMSE within  $\pm 5$  nm, suitable for process control in barrier film manufacturing. Three regression models—kNN, PCA Regression, and FFT-linear—demonstrate robust performance under substrate motion at speeds up to 12 m/min, validating compatibility with roll-to-roll production environments.

The modest accuracy degradation with decreasing resolution, combined with substantial computational savings, positions multispectral reflectometry as a viable alternative to full-spectrum approaches for inline metrology. Future deployment should prioritize spectral resolutions in the 50–100 nm range, leverage adaptive wavelength selection to optimize sensitivity, and incorporate active calibration monitoring to ensure long-term stability. These findings provide a pathway toward scalable, real-time thickness inspection for high-throughput nano-thin film manufacturing.

## ACKNOWLEDGMENTS

The authors acknowledge the University of Waterloo for research support. The authors thank Nfinite Nanotechnology for providing the ZnO-coated PLA samples used in this study and the IDEAs Clinic at the University of Waterloo for the tools and workspace used to build the apparatus. AI tools were used for language and grammar assistance during manuscript preparation and to accelerate coding. All technical analysis and scientific interpretation were performed by the authors.

## REFERENCES

1. K. Maize, Y. Mi, M. Cakmak, and A. Shakouri, “Real-time metrology for roll-to-roll and advanced inline manufacturing: A review,” *Advanced Materials Technologies* **8**(2), 2022.
2. E. Grau-Luque, M. Guc, I. Becerril-Romero, V. Izquierdo-Roca, A. Pérez-Rodríguez, P. Bolt, F. Van den Bruele, and U. Ruhle, “Thickness evaluation of AlO<sub>x</sub> barrier layers for encapsulation of flexible PV modules in industrial environments by normal reflectance and machine learning,” *Progress in Photovoltaics* **30**, pp. 229–239, 2021.
3. A. S. Yersak, Y. C. Lee, J. A. Spencer, and M. D. Groner, “Atmospheric pressure spatial atomic layer deposition web coating with in situ monitoring of film thickness,” *Journal of Vacuum Science and Technology A: Vacuum, Surfaces and Films* **32**(1), 2013.

4. A. Shan, M. Fried, G. Juhász, and C. Major, “High-speed imaging/mapping spectroscopic ellipsometry for in-line analysis of roll-to-roll thin-film photovoltaics,” *IEEE Journal of Photovoltaics* **4**(1), pp. 355–361, 2014.
5. H. G. Tompkins and E. A. Irene, *Handbook of Ellipsometry*, William Andrew Publishing, 2005.
6. H. Fujiwara, *Spectroscopic Ellipsometry: Principles and Applications*, John Wiley & Sons, 2007.
7. J. N. Hilfiker, G. K. Pribil, R. Synowicki, A. C. Martin, and J. S. Hale, “Spectroscopic ellipsometry characterization of multilayer optical coatings,” *Surface and Coatings Technology* **357**, pp. 114–121, 2019.
8. O. Stenzel and M. Ohlidal, eds., *Optical Characterization of Thin Solid Films*, vol. 64 of *Springer Series in Surface Sciences*, Springer International Publishing, Cham, Switzerland, 2018.
9. D. Aspnes, “The accurate determination of optical properties by ellipsometry,” in *Handbook of Optical Constants of Solid*, pp. 89–112, Academic Press, 1997.
10. M. Born and E. Wolf, *Principles of Optics: Electromagnetic Theory of Propagation, Interference and Diffraction of Light*, Cambridge University Press, Cambridge, UK, 7th ed., 1999.
11. R. Swanepoel, “Determination of the thickness and optical constants of amorphous silicon,” *Journal of Physics E: Scientific Instruments* **16**(12), pp. 1214–1222, 1983.
12. J. Liu, D. Zhang, D. Yu, M. Ren, and J. Xu, “Machine learning powered ellipsometry,” *Light: Science & Applications* **10**, 2021.
13. Zhang *et al.*, “Multi-wavelength spectrum reconstruction for thin film measurement,” *Optics Express* , 2024. Discrete multi-band reflectance inversion with polynomial reconstruction, 10 wavelengths.
14. P. Poodt, R. Knaapen, A. Illiberi, F. Roozeboom, and A. van Asten, “Low temperature and roll-to-roll spatial atomic layer deposition for flexible electronics,” *Journal of Vacuum Science and Technology A: Vacuum, Surfaces and Films* **30**(1), 2011.
15. D. Munoz-Rojas and J. MacManus-Driscoll, “Spatial atmospheric atomic layer deposition: a new laboratory and industrial tool for low-cost photovoltaics,” *Materials Horizons* **1**(3), pp. 314–320, 2014.
16. P. O. Oviroh, R. Akbarzadeh, D. Pan, R. A. M. Coetzee, and T. C. Jen, “New development of atomic layer deposition: processes, methods and applications,” *Science and Technology of Advanced Materials* **20**(1), pp. 465–496, 2019.
17. H. Asgarimoghaddam, Q. Chen, F. Ye, A. Shahin, B. Song, and K. P. Musselman, “Zinc aluminum oxide encapsulation layers for perovskite solar cells deposited using spatial atomic layer deposition,” *Small Methods* **8**(3), p. 2300995, 2024.
18. Lu *et al.*, “SNV/MSC normalization applied to reflectance data,” *Journal of Spectroscopy* , 2022. SNV (Standard Normal Variate) and MSC (Multiplicative Scatter Correction) preprocessing pipeline.
19. J. Bae, J. Park, H. Ahn, and J. Jin, “Optical method for simultaneous thickness measurements of two layers with a significant thickness difference,” *Optics Express* **29**, pp. 31615–31631, Sept. 2021.
20. A. S. Yersak, R. J. Lewis, J. Tran, and Y. C. Lee, “Characterization of thin film dissolution in water with in situ monitoring of film thickness using reflectometry,” *Applied Materials and Interfaces* **8**(27), pp. 17622–17630, 2016.
21. P. Hlubina, J. Lunacek, D. Ciprian, and R. Chlebus, “Spectral interferometry and reflectometry used to measure thin films,” *Applied Physics B* **92**, pp. 203–207, 2008.
22. Sánchez-Arriaga *et al.*, “Dual MEMS spectrometer reflectometry for inline thin film inspection,” *Sensors and Actuators* , 2023. Continuous-Frequency Method (CFM) and Interference Intensity Model (IIM), 10-20 ms measurement time.